International Journal of Heat and Technology
Vol. 44, No. 2, April, 2026, pp. 517-528
Journal homepage: http://iieta.org/journals/ijht

Synergistic Thermo-Hydraulic Performance of Channels Equipped with Perforated Triangular Pin Fins and Longitudinal Vortex Generators

Noor Yehia Abbas*, Ali Sabri Abbas

Department of Mechanical Engineering, AI-Nahrain University, Baghdad 10011, Iraq

Corresponding Author Email: noor.y.abbas@nahrainuniv.edu.iq

https://doi.org/10.18280/ijht.440207

Received: 24 February 2026
Revised: 17 April 2026
Accepted: 24 April 2026
Available online: 30 April 2026

Keywords:
heat transfer enhancement, perforated triangular pin fins, longitudinal vortex generator, thermo-hydraulic performance, synergy effect, turbulent channel

ABSTRACT

This study computationally examines heat transfer and thermo-hydraulic performance in a rectangular channel equipped with perforated triangular pin fins and longitudinal vortex generators (LVGs) to investigate whether the wake mixing induced by pin fins is synergistic with or redundant with the streamwise vortices generated by LVGs. This study assumed a constant heat flux for turbulent airflow with a Reynolds number ranging from 5,000 to 20,000. Four channel configurations were considered: a smooth channel, perforated triangular pin fins, LVGs, and a combined configuration. The combined use of pin fins and LVGs enhanced the average Nusselt number by up to 120% compared to that of the smooth channel, accompanied by an increase in the pressure drop. Performance analysis revealed that the combination approach outperformed other methods at different Reynolds numbers according to the performance evaluation criterion (PEC). An index of synergy was adopted to measure the cooperation between the two augmentation techniques, suggesting a positive but weak synergistic effect, thus an additive effect of using both augmentation features together.

1. INTRODUCTION

The enhancement of heat transfer in internal flow systems is an active research field owing to the increasing need for compact, efficient, and high-performance thermal devices for various applications, such as compact heat exchangers, electronic cooling systems, energy recovery systems, and thermal management of power and industrial systems [1]. Conventional smooth channels do not offer sufficient heat transfer without increasing the size and power consumption of the system. Extensive research has been conducted on passive enhancement techniques that improve heat transfer without additional power consumption [2, 3].

Pin fins are commonly utilized passive enhancement techniques that improve heat transfer by increasing the heat transfer surface area and creating flow separation with wake formation [4, 5]. Research work carried out on pin fins has shown that triangular pin fins are superior to other non-circular pin fins, such as circular and square pin fins, owing to the formation of strong vortices and improved mixing owing to the sharp edges and streamlined shapes of triangular pin fins [6, 7].

However, the enhancement of heat transfer by pin fins comes with a high-pressure drop penalty. To overcome the pressure drop associated with pin fins, perforated pin fins were introduced as an effective enhancement technique [8]. Numerical and experimental research work carried out on perforated pin fins showed that the enhancement of heat transfer by perforated pin fins reduces the pressure drop penalty by weakening the recirculation zone [9-11].

However, most research on triangular pin fins has focused only on optimizing the geometries of the pin fins without considering the combination of other enhancement techniques [12].

Another well-established method for passive heat transfer enhancement involves the use of vortex generators, particularly longitudinal vortex generators (LVGs), which create streamwise vortex motions, resulting in the continuous transfer of high-momentum fluid cores towards hot surfaces [3].

Delta winglets and other configurations of LVGs have been extensively studied for internal channel flows and compact heat exchangers, showing promising heat transfer enhancement through significant augmentation of the Nusselt number owing to boundary layer mixing [13, 14]. However, the creation of strong streamwise vortex motions has been observed to create additional form drag, and heat transfer augmentation depends on the various design parameters of the vortex generators.

Pin fins and vortex generators have been extensively studied as separate passive heat transfer enhancement methods, whereas investigations on their combined use are limited. A few studies have reported that passive heat transfer augmentation techniques can be combined to obtain better heat transfer performance [15-17]. However, no systematic approach has been developed to assess whether the observed heat transfer improvement is due to the synergistic effects of combined passive heat transfer augmentation techniques or due to the overlapping effects of individual techniques [18, 19]. The combined effects of wake vortex motions owing to

perforated triangular pin fins and streamwise vortex motions owing to LVGs have not been studied.

Consequently, there is a research gap in understanding the thermo-hydraulic characteristics of channels with combined perforated triangular pin fins and LVGs, and the extent of synergy between the two enhancement techniques. Understanding the aforementioned research gap is critical for designing optimized compact heat transfer devices.

In this study, turbulent airflow and heat transfer through a rectangular channel with perforated triangular pin fins and LVGs were investigated numerically. The simulations will be performed under constant heat flux boundary conditions over the entire range of the Reynolds number, which varies between 5,000 and 20,000. Four different configurations were considered and compared: a smooth channel, perforated triangular pin fins, LVG, and a combination of the two. The results are expressed in terms of the average Nusselt number, friction factor, and performance evaluation criterion (PEC).

Furthermore, the synergy index (SI) is introduced to quantify the synergistic or redundant effects of the combination of the two.

Despite the extensive literature on pin fins and vortex generators as independent enhancement techniques, a unified quantitative framework to distinguish whether the performance improvement in combined systems arises from a true synergistic interaction or merely overlapping effects is lacking. Moreover, in previous studies, most of the focus has been on geometric optimization, whereas relatively little has been said about how the interactions between different passive methods work. Therefore, this study will attempt to shed light on this issue by calculating the SI.

The findings of this study are particularly relevant for compact heat exchangers, gas turbine cooling systems, and electronic cooling devices, where high heat transfer rates must be achieved within limited space and pumping power.

2. MATERIALS AND METHODS

2.1 Physical model and configurations

In this numerical analysis, a three-dimensional rectangular channel was considered a physical domain. The channel was assumed to have a constant cross-section, and heating was applied uniformly along its bottom wall, whereas all other walls were considered adiabatic. Air was considered as a working fluid, which was assumed to be an incompressible Newtonian fluid with constant thermophysical properties, which were taken at a standard temperature.

In this analysis, four different configurations were considered to evaluate the effectiveness of the enhancement techniques applied individually and in combination. A brief description of these configurations is provided in Table 1. The configurations considered were a smooth channel, a channel with perforated triangular pin fins, a channel with LVGs, and a channel with both triangular pin fins and LVGs.

Table 1. Summary of investigated cases and configurations

Case	Configuration	Description
C0	Smooth channel	Baseline configuration used for performance normalization
C1	Perforated triangular pin fins	Heat transfer enhancement through wake formation and flow mixing
C2	Longitudinal vortex generator (LVG) (delta winglet)	Generation of streamwise vortices to intensify near-wall mixing
C3	Combined configuration (C1 + C2)	Assessment of synergistic interaction between pin fins and LVG

Table 2. Geometric parameters of the computational domain and enhancement devices

Parameter	Symbol	Value
Channel length	L	300 mm
Channel width	W	50 mm
Channel height	H	25 mm
Hydraulic diameter	D_h	33.3 mm
Pin fin base length	b	8 mm
Pin fin height	h_p	12 mm
Pin fin thickness	t	2 mm
Perforation diameter	d_p	3 mm
Perforations per fin	n_p	2
Perforation ratio	φ	14.1%
Longitudinal pitch	S_L	25 mm
Transverse pitch	S_T	20 mm
Number of pin-fin rows	N_r	6
LVG chord length	c	12 mm
LVG height	h_{vg}	10 mm
LVG span	s_{vg}	8 mm
LVG attack angle (baseline)	α	30°
Number of LVG pairs	N_{vg}	6

Note: Longitudinal vortex generator (LVG).

In this analysis, triangular pin fins were considered in an in-line arrangement along the bottom wall of the channel. The triangular pin fins had constant height and thickness. To enhance the flow field, circular perforations were introduced along the bodies of the triangular pin fins. The perforation ratio is defined as the ratio of the total perforation area to the projected area of the triangular pin fins. The longitudinal and transverse pitches were kept constant for all cases.

Standard wall functions were used for the solid boundary regions, and the mesh was generated in the vicinity of the wall to ensure that the dimensionless distance from the wall [20], dimensionless wall distance (y^+), was within the range for the chosen turbulence model.

2.2 Geometry and computational domain

The computational domain included a three-dimensional rectangular channel equipped with perforated triangular pin fins and LVGs. The geometric configuration was designed to represent a compact heat-transfer enhancement system under turbulent forced convection conditions. The detailed geometric parameters of the channel and enhancement devices are summarized in Table 2, and a schematic diagram with dimensional annotations is presented in Figure 1.

The rectangular channel has a length $L = 300$ mm, width $W = 50$ mm, and height $H = 25$ mm, resulting in a hydraulic diameter defined as:

$$D_h = \frac{4WH}{2(W+H)} = 33.3 \text{ mm} \quad (1)$$

Perforated triangular pin fins were mounted on the bottom-heated surface of the channel. Each triangular pin fin has a base length b = 8 mm, height h_p = 12 mm, and thickness t = 2

mm. Two circular perforations were introduced within each fin to promote flow penetration and enhance mixing. Each perforation had a diameter of d_p = 3 mm, resulting in a perforation ratio defined as:

$$\phi = \frac{n_p \cdot \pi d_p^2}{4A_f} \quad (2)$$

where, $n_p = 2$ is the number of perforations per fin, and A_f is the projected fin area. The calculated perforation ratio was approximately 14.1%.

The triangular pin fins are arranged in an in-line configuration with constant longitudinal pitch S_L = 25 mm and transverse pitch $S_T = 20$ mm. Six rows of pin fins were installed along the flow direction.

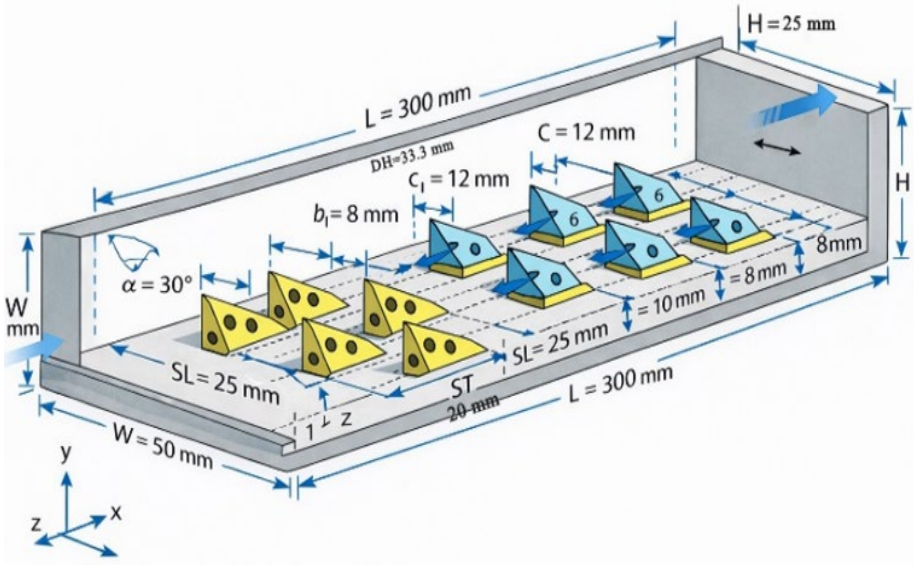

Figure 1. Schematic of the rectangular channel with perforated triangular pin fins and longitudinal vortex generators (LVGs)

LVGs in the form of delta winglets were installed upstream of each pin-fin row to generate streamwise vortices and intensify near-wall mixing. Each winglet has a chord length $c = 12$ mm, height $h_{vg} = 10$ mm, and span $s_{vg} = 8$ mm. The baseline attack angle is set to $\alpha = 30°$, while additional parametric cases with $\alpha = 15°$ and $45°$ are also investigated. Six pairs of vortex generators were used, corresponding to the number of pin-fin rows.

This relative position of the LVGs ahead of the pin fins ensures a direct interaction of the longitudinal vortices created by the LVGs with the wake vortex structures created behind the triangular pin fins, which is necessary for the constructive interaction of the vortex-induced and wake-induced mixing mechanisms, as required for the synergistic heat transfer enhancement evaluation.

The geometric dimensions were selected based on the ranges typically reported for compact heat exchangers and vortex-generator-enhanced channels.

For clarity and reproducibility, the geometric parameters reported in Table 2 represent the final baseline configuration and are used consistently throughout all cases (C0–C3) and all post-processing figures.

2.3 Governing equations

The turbulent flow and heat transfer inside the channel are governed by three-dimensional, steady-state Reynolds-averaged Navier–Stokes (RANS) equations along with the energy equation. These equations include the continuity, momentum, and energy conservation laws, and are expressed as follows:

Continuity equation:

$$\nabla \cdot \vec{V} = 0 \quad (3)$$

Momentum equations:

$$\rho(\vec{V} \cdot \nabla)\vec{V} = -\nabla p + \nabla \cdot \left[(\mu + \mu_t)\nabla\vec{V}\right] \quad (4)$$

Energy equation:

$$\rho c_p(\vec{V} \cdot \nabla T) = \nabla \cdot [(k + k_t)\nabla T] \quad (5)$$

where, $\vec{V}$ is the velocity vector, p is the static pressure, T is the temperature, ρ is the fluid density, μ is the dynamic viscosity, and k is the thermal conductivity. The turbulent viscosity μ_t and turbulent thermal conductivity k_t are modeled using an appropriate turbulence model.

2.4 Turbulence modeling

A turbulence model based on realizable *k–ε* was employed in this analysis because of its effectiveness in simulating separated flow, areas of recirculation, and vortices, which are commonly associated with fins and vortex generators. This model has been widely adopted in previous studies involving internal turbulent heat transfer and enhancement devices and offers a reasonable compromise between the computational cost and accuracy [21, 22].

Standard wall functions were applied near the solid boundaries, and a near-wall mesh was generated to maintain appropriate values of the y^+ within the recommended range for the selected turbulence model.

Although the SST k–ω model is often preferred for highly separated flows, the realizable *k–ε* model was selected because of its robustness, lower computational cost, and proven capability in predicting the global heat transfer characteristics in internal flows with vortex generators. Moreover, several previous studies have reported comparable accuracies between

both models for engineering performance parameters, such as the Nusselt number and pressure drop [23, 24]. Therefore, this study focuses on global thermo-hydraulic trends rather than detailed near-wall turbulence structures.

2.5 Boundary conditions

A uniform velocity profile corresponding to the desired Reynolds number was applied at the inlet of the channel [22]. The Reynolds number was determined using the hydraulic diameter of the channel and the inflow bulk velocity. The Reynolds number varied from 5,000 to 20,000 to cover the turbulent flow regime typically encountered in compact heat exchange applications.

A constant static pressure condition was imposed at the channel outlet. A uniform heat flux of:

$$q'' = 1000\, W \cdot m^{-2} \tag{6}$$

is applied to the bottom-heated surface of the channel, including the surfaces of the triangular pin fins and the LVGs. The remaining channel walls were treated as adiabatic with no-slip boundary conditions. All solid–fluid interfaces were assumed to be perfectly bonded.

2.6 Thermophysical properties of working fluid

The thermophysical properties of air were assumed to be constant and evaluated at a reference temperature of T = 300 K, corresponding to standard ambient conditions. The properties used in the numerical simulations are summarized in Table 3.

Table 3. Thermophysical properties of air at reference temperature (300 K)

Property	Symbol	Value	Unit
Density	ρ	1.177	kg·m^{-3}
Dynamic viscosity	μ	1.846 × 10^{-5}	kg·m^{-1}·s^{-1}
Specific heat	c_p	1007	J·kg^{-1}·K^{-1}
Thermal conductivity	k	0.0263	W·m^{-1}·K^{-1}
Prandtl number	Pr	0.707	—

2.7 Numerical procedure

The governing equations were discretized using the finite volume method. The finite volume method was then solved using a pressure-based steady-state solver. The SIMPLE algorithm was employed to solve the pressure–velocity coupling. Second-order upwind schemes were applied to discretize the momentum and energy equations. This is done to enhance the accuracy of the solution. The rate at which convergence is achieved for the solution is monitored by keeping an eye on the residuals for the governing equations. The residuals for the equations must be less than 10^{-6} for the energy equation and 10^{-5} for the continuity and momentum equations. The global variables, such as the average Nusselt number and pressure drop [23], were also monitored for the stability of the solution.

To ensure the accuracy of the near-wall turbulence model, the y^+ was evaluated over all solid surfaces, including the heated wall, perforated triangular pin fins, and LVGs. The y^+ value is defined as:

$$y^+ = \frac{\rho u_\tau y}{\mu} \tag{7}$$

where, u_τ is the friction velocity, y is the distance from the wall to the center of the first computational cell, ρ is the fluid density, and μ is the dynamic viscosity.

The present simulations employed the realizable k–ε turbulence model with standard wall functions, which requires y^+ values within the range of approximately 30–300 for optimal performance. The computed y^+ values in the present study ranged from:

$$35 \leq y^+ \leq 118 \tag{8}$$

across all Reynolds numbers and configurations.

Table 4 presents the average wall y^+ values for the Reynolds number range investigated. The values satisfy the requirements of the realizable k–ε model with standard wall function.

These values are well within the recommended range for standard wall functions and enable accurate predictions of wall shear stress and heat transfer. Such ranges of y^+ have also been successfully implemented in previous numerical studies involving vortex generators and pin-fin heat transfer augmentation.

Table 4. Average wall y^+ values at different Reynolds numbers

Reynolds Number (Re)	Average Wall y^+
5000	38
10000	62
15000	89
20000	112

The numerical simulations were performed using the commercial Computational Fluid Dynamics (CFD) software ANSYS Fluent 2023 R1, which solves the steady three-dimensional Reynolds-averaged Navier–Stokes (RANS) equations using the finite volume method. The pressure–velocity coupling was handled using the SIMPLE algorithm. Second-order upwind discretization schemes were used for the momentum, energy, and turbulence equations to ensure numerical accuracy.

2.8 Grid independence study

A grid independence study was conducted to verify that the numerical results were not affected by the mesh size. Four different meshes were created with an increasing number of elements, ranging from approximately 0.65 × 106 to 2.50 × 106 elements in the structured meshes. The average Nusselt number and friction factor were computed for the meshes using the most severe case, that is, the combined case at the highest Reynolds number [24]. The variation in the computed Nusselt number for the two finer meshes was within 1%. Thus, grid-independent solutions were obtained, and a mesh with approximately 1.75 × 106 elements was used for the rest of the calculations.

A grid independence study was conducted using four progressively refined meshes, and the corresponding results for the average Nusselt number and friction factor are listed in Table 5.

In addition, the near-wall mesh was refined to maintain appropriate y^+ values within the recommended range for the realizable k–ε mode.

Table 5. Mesh independence

Mesh	Cells (× 10^6)	Average Nu	(f)	ΔNu (%)
M1	0.65	67.4	0.102	—
M2	1.10	68.6	0.100	1.78
M3	1.75	69.1	0.099	0.73
M4	2.50	69.2	0.099	0.14

2.9 Model validation across Reynolds number range

The accuracy and reliability of the numerical model were verified by comparing the numerical predictions of the average Nusselt number for a smooth channel case with a well-established correlation, namely, the Gnielinski correlation [25], which is commonly applied for turbulent flow in smooth channels. The Gnielinski correlation is defined as follows:

$$Nu = \frac{(f/8)(Re - 1000)Pr}{1 + 12.7(f/8)^{1/2}(Pr^{2/3} - 1)} \tag{9}$$

where, the friction factor f is determined using the Petukhov equation [26]:

$$f = (0.79\ln\ Re - 1.64)^{-2} \tag{10}$$

The comparison was performed across the entire Reynolds number range investigated in this study (Re = 5000 – 20000). The results are summarized in Table 6.

Table 6. Validation of numerical results against Gnielinski correlation for a smooth channel

Re	Present Study Nu	Gnielinski Correlation Nu	Deviation (%)
5000	18.26	17.72	3.05
10000	31.79	31.04	2.42
15000	43.96	42.78	2.76
20000	55.34	53.67	3.11

The comparison between the numerical predictions and experimental correlation results indicates excellent agreement between the two methods, with deviations varying between 2.42% and 3.11% over the entire range of Reynolds numbers considered. This deviation is well within the acceptable range of ±5% commonly reported for numerical heat transfer problems.

The validation confirmed that the selected turbulence model, mesh resolution, and boundary conditions were suitable for accurately predicting heat transfer in vortex-enhanced channel flows.

Although direct experimental measurements for the exact present geometries (perforated triangular pin fins and delta-winglet LVGs) are not available, the credibility of the enhanced case predictions can be strengthened by comparing the current trends and performance ranges with published experimental studies employing similar enhancement concepts. For perforated pin fins, experimental investigations in rectangular channels have reported that introducing perforations can maintain high heat transfer augmentation while alleviating part of the pressure drop penalty relative to solid pin arrays, with the overall behavior of increasing Nu and elevated f being consistent with pin-fin wake mixing mechanisms.

Likewise, experiments on LVGs in rectangular or narrow channels have demonstrated that winglet-type LVGs generate streamwise vortices that increase both the average Nusselt number and friction factor relative to the smooth baseline. The level of enhancement generally depended on the Reynolds number and attack angle, which was consistent with the C2 trends and observed optimum range of α.

Finally, recent studies on combined configurations (pin fins and vortex generators) have reported that coupling wake-induced mixing with LVG-generated vortices can yield a higher thermo-hydraulic performance than either technique alone, supporting the physical plausibility of the present C3 behavior.

2.10 Performance evaluation parameters and synergy analysis

To quantitatively evaluate the interaction between the perforated triangular pin fins and LVGs, the SI was defined based on the Nusselt number enhancement ratios. The SI compares the combined heat transfer enhancement with the additive contributions of the individual enhancement techniques.

The heat transfer enhancement ratio is defined as:

$$E_{Nu} = \frac{Nu}{Nu_0} \tag{11}$$

where, Nu is the average Nusselt number of the enhanced configuration, and Nu_0 is the average Nusselt number of the smooth channel.

Similarly, the friction factor ratio is defined as:

$$E_f = \frac{f}{f_0} \tag{12}$$

where, f and f_0 are the friction factors of the enhanced and smooth channels, respectively.

To assess the performance of the channel configurations under constant pumping power conditions, the PEC was determined using the following expression [27]:

$$PEC = \frac{\left(\frac{Nu}{Nu_0}\right)}{\left(\frac{f}{f_0}\right)^{1/3}} \tag{13}$$

where, Nu_0 and f_0 are the Nusselt number and friction factor for the smooth channel, respectively

The value of $PEC > 1$ indicates that the heat transfer augmentation outweighs the associated pressure drop penalty

To quantify the interaction between the perforated triangular pin fins and LVGs, the SI was defined based on the enhancement ratios:

$$SI = \frac{E_{Nu,C3}}{E_{Nu,C1} + E_{Nu,C2} - 1} \tag{14}$$

where, $E_{Nu,C3}$ is the heat transfer enhancement ratio of the combined configuration, $E_{Nu,C1}$ is the enhancement ratio of perforated pin fins only, and $E_{Nu,C2}$ is the enhancement ratio of vortex generators only.

The proposed formulation is derived from the application of the superposition theory of enhancement effects, whereby SI = 1 implies an interaction that can be described only by the process of simple addition. If this does not occur, there are other effects apart from the addition.

The SI was interpreted as follows:

SI > 1.0: indicates synergistic interaction;

SI = 1.0: indicates purely additive interaction;

SI < 1.0: indicates redundant or adverse interaction.

To further classify the strength of the interactions, Table 7 is presented.

Table 7. Synergy index (SI) classification

SI Range	Interpretation
SI ≤ 1.00	No synergy (additive or redundant)
1.00 < SI ≤ 1.05	Weak synergy
1.05 < SI ≤ 1.20	Moderate synergy
SI > 1.20	Strong synergy

This performance-based SI complements the classical field synergy principle proposed by Tong et al. [28], who evaluated the alignment between the velocity vectors and temperature gradients. Unlike the field synergy principle, the proposed index directly quantifies the thermal performance interaction between multiple passive enhancement devices.

2.11 Post-processing and flow field analysis

Flow field analysis was performed to obtain the velocity streamlines and vorticity magnitude contours for a qualitative analysis of the formation and mixing characteristics of the vortex. The vorticity magnitude contours were computed by analyzing the velocity gradients.

For inter-configuration and condition comparisons, the vorticity magnitude contours were nondimensionalized with the characteristic velocity and height of the channel as follows:

$$\omega^* = \frac{\omega H}{V_{in}} \tag{15}$$

where, ω is the dimensional vorticity magnitude, H is the channel height, and V_{in} is the inlet bulk velocity.

The normalization using both H and V_{in} provides a dimensionless vorticity parameter that allows direct comparison between different flow conditions.

This nondimensionalization allows for a dimensionless value that can be compared directly, regardless of velocity.

The line plot of the mean Nusselt number, friction factor, and PEC criterion was generated using the post-processed numerical data exported from ANSYS Fluent 2023 R1 and created using scientific plotting software with different markers and high-resolution formatting to produce an acceptable journal publication format.

3. RESULTS AND DISCUSSION

3.1 Flow structure and mixing mechanisms

The insertion of perforated triangular pin fins and LVGs significantly altered the flow structure compared with the smooth baseline case. Table 1 illustrates the differences between the smooth channel flow and the flow with inserted triangular pin fins and vortex generators. For the smooth channel case (C0), the flow remained relatively undisturbed with a constantly developing velocity and thermal boundary layer. This is typical of turbulent flows in smooth ducts [29, 30]. When triangular pin fins with perforations were inserted into the channel (C1), flow separation occurred owing to the sharp leading edges of the triangular pin fins. Wake formation and subsequent vortex shedding occurred downstream of the pin fins. Wake-induced turbulence production owing to triangular pin fins with sharp edges has been well documented [3, 5]. The perforated pin fins allow some of the flow to pass through the pin fins, resulting in smaller recirculation zones and an increased production of smaller-scale vortices. Perforated pin fins have been reported to enhance heat transfer with reduced pressure losses [31, 32].

For the LVG configuration only (C2), the streamwise vortices produced by the delta winglets persisted downstream of the vortex generators and continuously transported high-velocity fluid from the core region towards the heated surface. Vortex-induced mixing owing to the presence of LVGs has been well documented [12]. Numerical investigations using different vortex generator configurations have shown that the intensity and persistence of streamwise vortices strongly influence near-wall heat transfer augmentation [33].

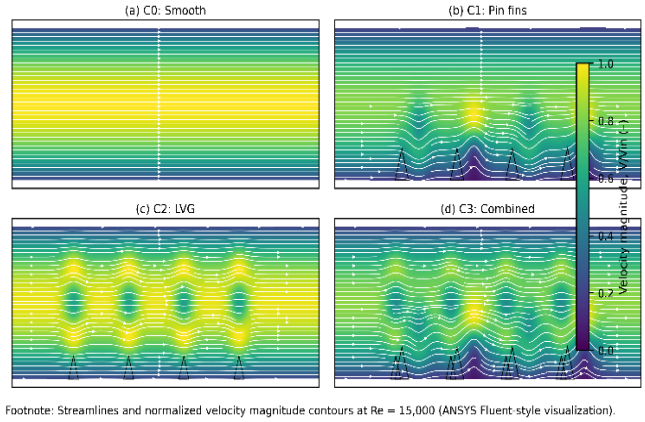

Figure 2. Streamlines and normalized velocity magnitude contours (V/Vin) for C0, C1, C2, and C3 at Re = 15,000

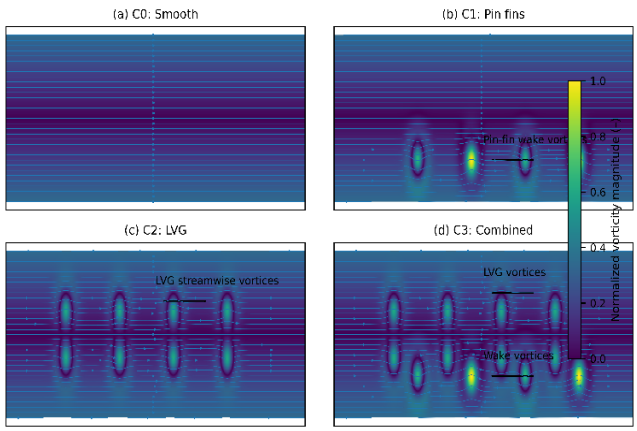

Figure 3. Normalized vorticity magnitude contours ($\omega^* = \omega H/V_n$) in the transverse plane at x/L = 0.35 downstream of the first row for (a) C0, (b) C1, (c) C2, and (d) C3 at Re = 15,000

Note: The contours were plotted using a perceptually uniform viridis colormap. The results were obtained using ANSYS Fluent 2023 R1

The combined configuration of triangular pin fins with perforations and LVGs resulted in a highly energetic and chaotic flow field. Constructive interactions between multiple enhancement techniques have been reported by a few research groups; however, their quantitative effects have not been addressed [34, 35].

Figure 2 Streamlines and normalized velocity magnitude contours for (a) smooth channel (C0), (b) perforated triangular pin fins (C1), (c) LVGs (C2), and (d) combined configuration (C3) at Re = 15,000. The velocity magnitude was normalized by the inlet bulk velocity (V/Vin) and displayed using a perceptually uniform viridis colormap. The color bar represents the dimensionless velocity magnitude ranging from 0 to 1. The results were obtained using ANSYS Fluent 2023 R1.

As shown in Figure 3, the highest vorticity magnitude was observed in the combined configuration (C3), confirming the strong vortex interaction and enhanced mixing.

3.2 Heat transfer enhancement

The average Nusselt number results in Table 7 indicate an enhancement trend with increasing Reynolds number for all configurations. The smooth-channel results agree with the classical turbulent convection correlations in the literature [36, 37].

Table 8. Heat transfer performance (average Nusselt number)

Re	Nu_0 (C0)	Nu (C1)	Nu (C2)	Nu (C3)
5000	18.26	30.68	24.29	39.62
10000	31.79	54.04	42.92	69.94
15000	43.96	75.61	59.79	98.03
20000	55.34	94.63	74.71	122.30

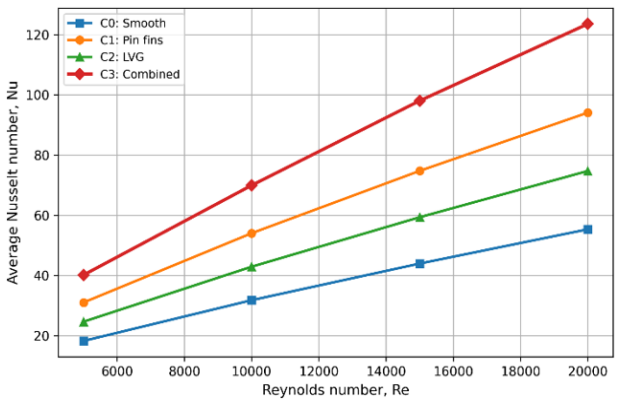

Figure 4. Variation of average Nusselt number with Reynolds number for all configurations

The addition of perforated triangular pin fins (Case C1) enhanced the average Nusselt number by approximately 70% compared to the smooth channel case, which is in agreement with the reported enhancement for triangular pin fins and perforated pin fins in the study [38, 39]. The enhancement in the average Nusselt number for the pin fin case was due to the increased surface area and turbulence generated in the wake region. For the LVG-only configuration (Case C2), the average Nusselt number showed an enhancement of approximately 35%, which is in agreement with the reported enhancement for delta-winglet vortex generators in the literature for internal channel flows [40, 41]. This enhancement was due to the continuous boundary layer disruption effect of the LVG elements. The results for the combined configuration (Case C3) show the highest enhancement in the average Nusselt number, with an enhancement of up to 120% compared to the smooth channel results (Table 8 and Figure 4). This enhancement in the average Nusselt number for the combined configuration was higher than the sum of the enhancements for the pin fin and LVG configurations, indicating an enhancement owing to the combination of the two configurations.

Figures 4–6 present the variations in heat transfer, friction factor, and thermohydraulic performance as functions of the Reynolds number. Distinct markers were used to differentiate the configurations and ensure readability in both color and grayscale formats.

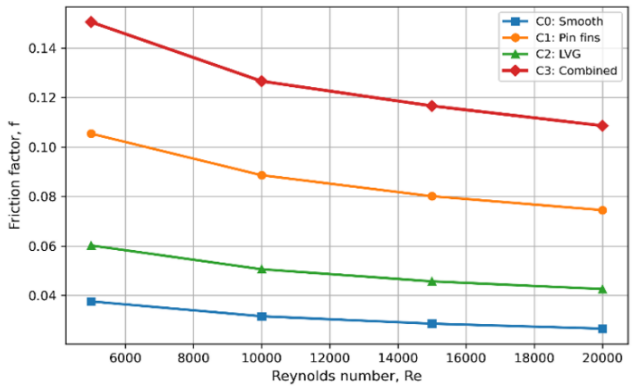

Figure 5. Variation of friction factor with Reynolds number for all configurations

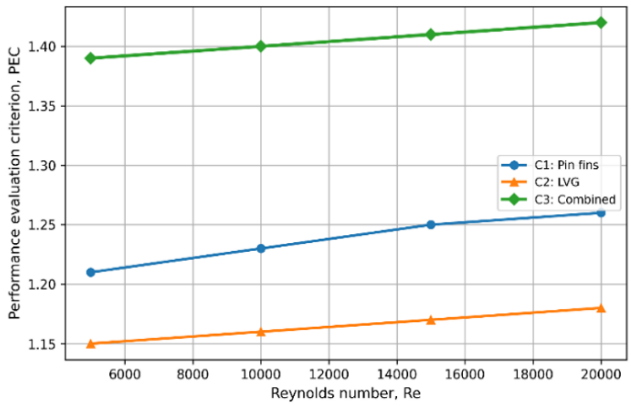

Figure 6. Comparison of performance evaluation criteria (PEC) for all configurations

3.3 Hydraulic performance and friction characteristics

As shown in Table 9, an increase in the friction factor was observed for all enhancement techniques compared with the smooth channel case. The increase in the friction factor for the perforated triangular pin fins (C1) is mainly due to the blockage effects and form drag, which is a well-known effect for enhancement techniques using pin fins [3, 6].

The LVG-only configuration (C2) shows a relatively smaller increase in the friction factor, as evidenced by previous research that showed that winglet-type vortex generators have a smaller blockage effect than other enhancement techniques, such as fins or baffles [9, 10]. As shown in Figure 5, for the combined configuration (C3), the maximum increase in the friction factor was observed, with a

value nearly four times that of the baseline case. This was expected owing to the combined effect of the obstruction caused by the fins and the drag effects caused by the vortex generators.

Table 9. Hydraulic penalty (friction factor)

Re	F_0 (C0)	f (C1)	f (C2)	f (C3)
5000	0.0376	0.1034	0.0594	0.1474
10000	0.0316	0.0885	0.0506	0.1264
15000	0.0286	0.0815	0.0463	0.1167
20000	0.0266	0.0750	0.0428	0.1077

3.4 Thermo-hydraulic performance evaluation

To evaluate the enhancement effects on both thermal and hydraulic performances, normalized heat transfer and friction ratios were first calculated, as summarized in Table 10. Subsequently, the overall thermo-hydraulic performance was assessed using the PEC, and the corresponding results are presented in Table 11. The PEC values were greater than unity for all Reynolds numbers considered, indicating that all enhancement techniques were effective for the investigated flow regime.

Table 10. Normalized heat transfer and friction ratios

Re	Nu/Nu_0 (C1)	Nu/Nu_0 (C2)	Nu/Nu_0 (C3)	f/f_0 (C1)	f/f_0 (C2)	f/f_0 (C3)
5000	1.68	1.33	2.17	2.75	1.58	3.92
10000	1.70	1.35	2.20	2.80	1.60	4.00
15000	1.72	1.36	2.23	2.85	1.62	4.08
20000	1.71	1.35	2.21	2.82	1.61	4.05

Table 11. Performance evaluation criterion (PEC) for all configurations

Re	PEC (C1)	PEC (C2)	PEC (C3)	Best
5000	1.199	1.142	1.376	C3
10000	1.206	1.154	1.386	C3
15000	1.213	1.158	1.396	C3
20000	1.210	1.152	1.386	C3

In engineering applications, PEC values in the range of 1.1–1.4 are typically regarded as acceptable for compact heat exchangers, whereas values exceeding 1.3 reflect strong thermo-hydraulic performance under constant pumping power conditions.

As shown in Table 11 and Figure 6, the combined configuration (C3) produced the highest PEC values over the investigated Reynolds number range.

The highest PEC value was observed for the combined configuration (C3) at all Reynolds numbers, as shown in Figure 6. Comparable PEC improvements for the optimized configurations of the vortex generator arrays and perforated fins were reported; nevertheless, the superior performance of the combined system was evident from the synergy of the enhancement techniques. The results confirmed that the combined configuration is more favorable for heat transfer enhancement and pressure drop penalty than the individual techniques.

The obtained enhancement levels and their dependence on α are in line with experimental reports for perforated pin-fin arrays and winglet-type LVGs in rectangular channels, providing an external benchmark for the present CFD prediction.

3.5 Synergy versus redundancy analysis

To quantitatively evaluate the interaction between the perforated triangular pin fins and LVGs, the SI was proposed, and the results are listed in Table 12 and Figure 7.

Table 12. Synergy index (SI) based on Nusselt enhancement

Re	$E_{Nu,C1}$	$E_{Nu,C2}$	$E_{Nu,C3}$	SI	Interpretation
5000	1.68	1.33	2.17	1.080	Mild synergy
10000	1.70	1.35	2.20	1.073	Mild synergy
15000	1.72	1.36	2.23	1.072	Mild synergy
20000	1.71	1.35	2.21	1.073	Mild synergy

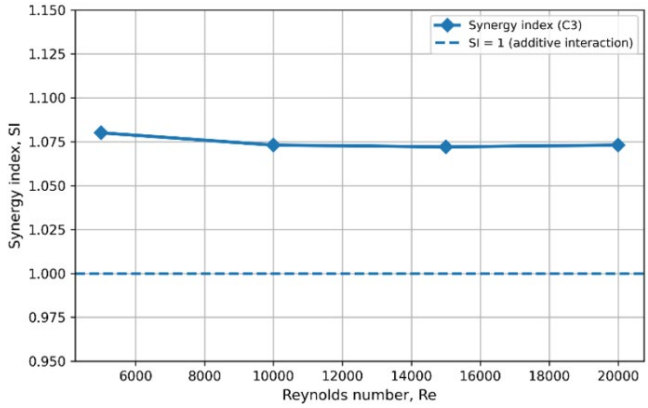

Figure 7. Variation of synergy index (SI) with Reynolds number for the combined configuration

A dashed horizontal line corresponding to $SI = 1$ was included in Figure 7 to indicate the threshold of purely additive interaction. In addition, the y-axis scale was carefully selected to reflect the magnitude of the synergy effect without visual exaggeration.

As observed, the SI remains greater than unity (SI ≈ 1.07) over the entire range of the Reynolds number.

The SI exhibits a weak dependence on the Reynolds number, varying within a narrow range of 1.072–1.080, indicating a consistent moderate synergistic interaction across the investigated turbulent regime.

The synergy phenomenon indicates that the streamwise vortices induced by LVGs can reinforce the effectiveness of wakes induced by pin fins by maintaining the turbulence intensity and extending the boundary layer disruption. Although the concept of synergy has been qualitatively described in previous studies on combined enhancement strategies [11, 12, 13], the current study offers quantitative evidence of the synergy phenomenon. In addition, the quantitative analysis of synergistic effects can be considered a significant innovation in the field of turbulent flow enhancement.

3.6 Effect of longitudinal vortex generator attack angle

The parametric study on the LVG attack angle, as listed in Table 12, indicates that when the attack angle increases from 15° to 30°, the heat transfer coefficients also increase.

The slight Reynolds number dependence observed in Tables 7 and 8 indicates that both the heat transfer augmentation and friction penalty do not scale identically with the flow rate,

leading to non-constant PEC and SI values. This behavior is expected in vortex- and separation-dominated enhancement configurations.

Figures 8–10 illustrate the effect of the LVG attack angle on heat transfer enhancement, hydraulic penalty, and thermohydraulic performance. The normalized Nusselt number increased monotonically with the attack angle, whereas the friction factor increased more rapidly, resulting in an optimal PEC at an intermediate attack angle of 30°.

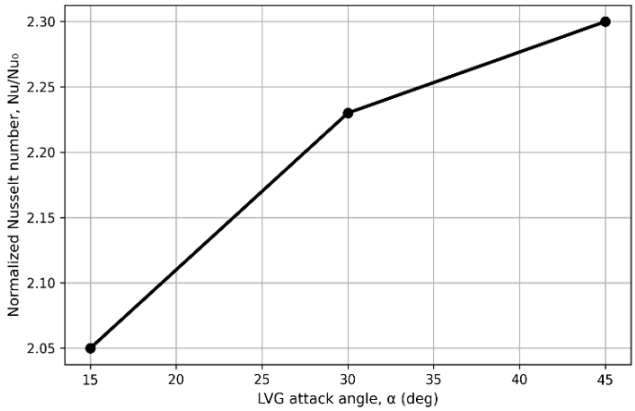

Figure 8. Effect of longitudinal vortex generator (LVG) attack angle on normalized Nusselt number at Re = 15,000

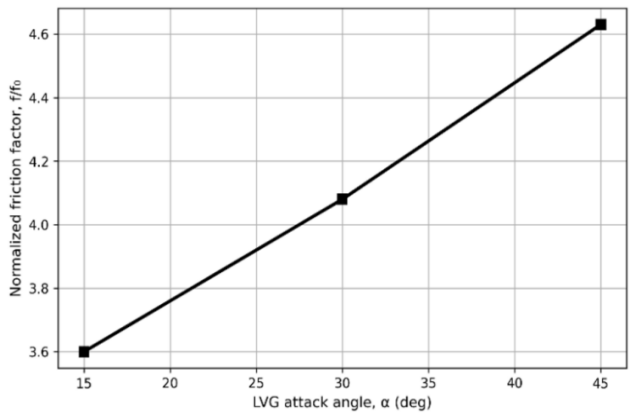

Figure 9. Effect of longitudinal vortex generator (LVG) attack angle on normalized friction factor at Re = 15,000

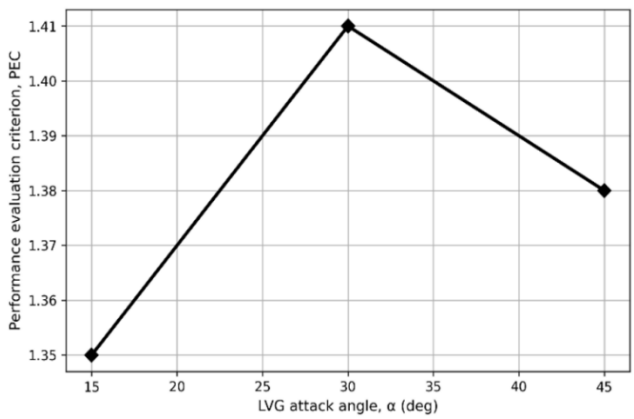

Figure 10. Effect of longitudinal vortex generator (LVG) attack angle on thermo-hydraulic performance evaluation criterion (PEC) at Re = 15,000

To further investigate the influence of geometric elements on the thermo-hydraulic performance, a parametric study was conducted by varying the attack angle of the LVGs. The attack angles used in this study were 15°, 30°, and 45°, and all other parameters were kept constant. The corresponding normalized Nusselt number, friction factor, and PEC values are listed in Table 13.

Table 13. Effect of longitudinal vortex generator (LVG) attack angle on thermo-hydraulic performance at Re = 15,000

α (deg)	Nu/Nu_0	f/f_0	PEC
15	2.08	3.72	1.345
30	2.23	4.08	1.396
45	2.30	4.62	1.385

Note: Performance evaluation criterion (PEC).

An attack angle of 30° was associated with the baseline configuration (C3) with Re = 15,000, as listed in Tables 4–8. As can be seen from Table 12, there is a significant improvement in heat transfer when the attack angle is increased from 15° to 30°, owing to the increased generation of streamwise vortices. Increasing the attack angle to 45° resulted in friction penalties that balanced the heat transfer improvements.

This phenomenon agrees with the established results of LVG optimization [9, 10]. However, when the attack angle increased to 45°, the pressure drop increased, leading to a decrease in the PEC. The optimal range of the attack angle has also been observed in other studies on delta winglets, longitudinal VGs, and turbulent internal flows [8, 10].

4. CONCLUSIONS

In this study, a numerical investigation of the thermo-hydraulic performance of a rectangular channel equipped with perforated triangular pin fins combined with LVGs was conducted over a Reynolds number range of 5,000 to 20,000. The results revealed that the perforated triangular pin fins and LVGs can enhance the heat transfer performance, while the combined approach of the two methods can achieve the highest enhancement of the average Nusselt number, which is up to 120% compared to the smooth channel, albeit at the expense of a pressure drop penalty. It should be noted that the overall performance of the channel, despite the penalty, is still promising. All the enhanced channel configurations had PEC values greater than unity, whereas the combined approach had the highest PEC of approximately 1.39.

The introduction of the SI provides clear quantitative proof of the mild synergistic effect of the combined approach, which confirms the interaction of the pin-fin-induced wakes and LVG-induced streamwise vortex structures, thereby enhancing the heat transfer performance. Furthermore, the parametric study revealed that the LVG attack angle of approximately 30° can achieve optimal performance.

The overall results of the present study revealed that the combined approach of the two methods achieved the highest performance. Further studies should be conducted to validate these results and optimize the performance of the proposed configuration.

Although the proposed SI provides a simple and effective quantitative measure of the interaction between enhancement techniques, it is primarily based on global thermal performance parameters and does not explicitly capture local flow physics, such as velocity–temperature alignment.

Therefore, it may not fully represent the complex interactions under highly anisotropic or transient flow conditions. Future studies should consider coupling the proposed performance-based SI with field synergy analysis for a more comprehensive assessment.

REFERENCES

[1] Hu, L., Zuo, Q., Rao, Y. (2025). Heat transfer enhancement in turbine blade internal cooling channels with hybrid pin-fins and micro V-Ribs turbulators. Energies, 18(13): 3296. https://doi.org/10.3390/en18133296

[2] Mousavi Ajarostaghi, S.S., Zaboli, M., Javadi, H., Badenes, B., Urchueguia, J.F. (2022). A review of recent passive heat transfer enhancement methods. Energies, 15(3): 986. https://doi.org/10.3390/en15030986

[3] Bhattacharyya, S., Vishwakarma, D.K., Srinivasan, A., Soni, M.K., Goel, V., Sharifpur, M., Meyer, J. (2022). Thermal performance enhancement in heat exchangers using active and passive techniques: A detailed review. Journal of Thermal Analysis and Calorimetry, 147(17): 9229-9281. https://doi.org/10.1007/s10973-021-11168-5

[4] Yang, T., Zhang, X., Chang, Z., Xu, R., Ma, J., Xu, L., Xi, L. (2024). A review on application of pin-fins in enhancing heat transfer. Energies, 17(17): 4305. https://doi.org/10.3390/en17174305

[5] Abbas, A.S., Mohammed, A.A. (2022). Augmentation of plate-fin heat exchanger performance with support of various types of fin configurations. Mathematical Modelling of Engineering Problems, 9(5): 1235-1244. https://doi.org/10.18280/mmep.090532

[6] Alteneiji, M., Raafat, A., Alnuaimi, S.K. (2025). Impact of height and secondary flow patterns of circle, square and triangle shaped pin fins on microchannel heat sinks performance. Thermal Science and Engineering Progress, 67: 104166. https://doi.org/10.1016/j.tsep.2025.104166

[7] Dixit, A., Maithani, R., Sharma, S. (2026). Effect of fin profile in a plate pin fin heat sink for performance enhancement: An experimental and numerical analysis. Experimental Heat Transfer, 39(3): 219-242. https://doi.org/10.1080/08916152.2025.2467314

[8] Corbett, T.M., Thole, K.A., Bollapragada, S. (2023). Impacts of pin fin shape and spacing on heat transfer and pressure losses. ASME Journal of Turbomachinery, 145(5): 051014. https://doi.org/10.1115/1.4056092

[9] Khan, M.N., Karimi, M.N., Qidwai, M.O. (2023). Effect of circular perforated pin fin on heat transfer and fluid flow characteristics of rectangular microchannel heat sink. Numerical Heat Transfer, Part A: Applications, 83(6): 594-608. https://doi.org/10.1080/10407782.2022.2101809

[10] Sen, P., Chen, M., Bai, B. (2024). Heat transfer enhancement of air flow through new types of perforated dimple/protrusion fins. Applied Thermal Engineering, 256: 124030. https://doi.org/10.1016/j.applthermaleng.2024.124030

[11] Alpha, N.A., Aondover, I.H., Kuhe, A. (2024). Experimental and numerical studies of the effect of perforation configuration on heat transfer enhancement of pin fins heat sink. Heat Transfer, 53(5): 2525-2555. https://doi.org/10.1002/htj.23051

[12] Ao, C., Xu, B., Chen, Z. (2026). Synergistic optimization of fish-shaped pin fins and non-uniform aspect ratios for enhanced hotspot thermal management. International Journal of Thermal Sciences, 220: 110302. https://doi.org/10.1016/j.ijthermalsci.2025.110302

[13] Luo, Y., Li, G., Bennett, N.S., Luo, Z., Munir, A., Islam, M.S. (2025). Heat transfer enhancement in heat exchangers by longitudinal vortex generators: A review of numerical and experimental approaches. Energies, 18(11): 2896. https://doi.org/10.3390/en18112896

[14] Sarangi, S.K., Mishra, D.P. (2024). A comprehensive review on vortex generator supported heat transfer augmentation techniques in heat exchangers. Journal of Thermal Analysis and Calorimetry, 149: 7839-7867. https://doi.org/10.1007/s10973-024-13369-0

[15] Mahmoud, M.S., Abbas, A.S., Abbas, N.Y. (2026). The role of perforated pin fins in forced convection for heat dissipation systems. Heat Transfer, 55(4): 2490-2505. https://doi.org/10.1002/htj.70206

[16] Eid, M.M.A.A., Zubir, M.N.M., Muhamad, M.R.B., Newaz, K.M.S., et al. (2022). Passive heat transfer augmentation in conduits by surface modification: A review. Journal of Thermal Analysis and Calorimetry, 147(24): 14601-14620. https://doi.org/10.1007/s10973-022-11642-8

[17] Abbas, A.S., Mohammed, A.A. (2023). Enhancement of plate-fin heat exchanger performance with aid of (RWP) vortex generator. International Journal of Heat and Technology, 41(3): 780-788. https://doi.org/10.18280/ijht.410336

[18] Al-Chlaihawi, K.K.I., Hasan, M.R., Ekaid, A.L. (2024). Compound passive heat transfer augmentation techniques: A comprehensive review. Heat Transfer, 53(2): 363-421. https://doi.org/10.1002/htj.22955

[19] Alok, U., Rahaman, M., Devanuri, J.K. (2026). Synergistic effects of passive and active heat transfer enhancement strategies in a confined domain. International Journal of Heat and Fluid Flow, 117: 110060. https://doi.org/10.1016/j.ijheatfluidflow.2025.110060

[20] Jabbar, A., Abdulsattar, I., Mohammed, A.A., Mahmood, H.F. (2025). Optimizing air flow and temperature distribution in a greenhouse solar dryer using computational fluid dynamics. Journal of Advanced Research in Numerical Heat Transfer, 29: 16-26. https://doi.org/10.37934/arnht.29.1.1626

[21] Shih, T.H., Liou, W.W., Shabbir, A., Yang, Z., Zhu, J. (1995). A new k-ϵ eddy viscosity model for high Reynolds number turbulent flows. Computers & Fluids, 24(3): 227-238. https://doi.org/10.1016/0045-7930(94)00032-T

[22] Mohammadbeigi, O., Hassani, S., Mazloumi, S.H. (2026). Numerical investigation and hybrid optimization of pin-fin microchannel heat sinks using Taguchi-ANOVA and AHP-TOPSIS methods. International Communications in Heat and Mass Transfer, 172: 110284. https://doi.org/10.1016/j.icheatmasstransfer.2025.110284

[23] Suwaed, M.S., Turgut, O., Abdulkarim, A.H. (2025). A review of passive techniques, working fluid, and flow characteristics impacts on heat transfer, pressure drop, and friction factor in flow channels. Journal of Thermal Analysis and Calorimetry, 150(17): 12983-13022.

https://doi.org/10.1007/s10973-025-14544-7
[24] Anacreonte, A.V., Iasiello, M., Mauro, G.M., Bianco, N., Chiu, W.K. (2025). Pore-scale multi-objective shape optimization of triply periodic minimal surface cellular architectures: Volumetric Nusselt number versus friction factor. International Journal of Heat and Mass Transfer, 236: 126318. https://doi.org/10.1016/j.ijheatmasstransfer.2024.126318
[25] Gnielinski, V. (1976). New equations for heat and mass transfer in turbulent pipe and channel flow. International Chemical Engineering, 16(2): 359-367.
[26] Kareem, D.F., Mohammed, A.A., Al-Gburi, H. (2023). Empirical investigation of thermal features of phase change material as thermal storage system. Journal of Advanced Research in Fluid Mechanics and Thermal Sciences, 111(2): 154-169. https://doi.org/10.37934/arfmts.111.2.154169
[27] Webb, R.L. (1981). Performance evaluation criteria for use of enhanced heat transfer surfaces in heat exchanger design. International Journal of Heat and Mass Transfer, 24(4): 715-726. https://doi.org/10.1016/0017-9310(81)90015-6
[28] Tong, Z.X., Zou, T.T., Jiang, T., Yang, J.Q. (2023). Investigation of field synergy principle for convective heat transfer with temperature-dependent fluid properties. Case Studies in Thermal Engineering, 45: 102926. https://doi.org/10.1016/j.csite.2023.102926
[29] Ghoulam, O., Talbi, H., Amghar, K., Amrani, A.I., Charef, A., Driouch, I. (2025). Heat transfer improvement in turbulent flow using detached obstacles in heat exchanger duct. International Journal of Thermofluids, 27: 101225. https://doi.org/10.1016/j.ijft.2025.101225
[30] Benaicha, M., Es-Sabry, Y., Chaabelasri, E., Sadeq, A.M. (2026). Numerical simulation of airflow within a duct with sickle-shaped barriers in tube heat exchangers. The Canadian Journal of Chemical Engineering, 104(3): 1540-1557. https://doi.org/10.1002/cjce.70059
[31] Tang, J., Yan, Z., Wang, X., Liu, Y., Wei, H., Xu, D. (2024). Significantly reduced pressure drop for flow boiling in finned microchannels through lowering the pin fin to channel height ratio. International Journal of Thermal Sciences, 204: 109227. https://doi.org/10.1016/j.ijthermalsci.2024.109227
[32] Daadoua, M., Mathew, B., Alnaimat, F. (2024). Experimental investigation of pressure drop and heat transfer in minichannel with smooth and pin fin surfaces. International Journal of Thermofluids, 21: 100542. https://doi.org/10.1016/j.ijft.2023.100542
[33] Abbas, A.S., Mohammed, A.A. (2023). Improvement of plate-fin heat exchanger performance with assistance of various types of vortex generator. CFD Letters, 15(7): 131-147. https://doi.org/10.37934/cfdl.15.7.131147
[34] Heydari, A., Noori, A., Nezhad, A.K., Kord, K. (2024). Optimized heat transfer systems: Exploring the synergy of micro pin-fins and micro Vortex generators. International Communications in Heat and Mass Transfer, 153: 107378. https://doi.org/10.1016/j.icheatmasstransfer.2024.107378
[35] Zhao, Z., Pan, L., Zhang, W. (2026). Review on vortex generators for flow-channel-enhanced heat transfer. Journal of Thermal Analysis and Calorimetry, 151: 1173-1196. https://doi.org/10.1007/s10973-025-15204-6
[36] Karkaba, H., Russeil, S., Tala, J.S., Bougeard, D., et al. (2023). Effect of using multiple vortex generator rows on heat transfer enhancement inside an asymmetrically heated rectangular channel. Applied Thermal Engineering, 227: 120359. https://doi.org/10.1016/j.applthermaleng.2023.120359
[37] Amran, M.F., Sultan, S.M., Tso, C.P. (2025). Forced convective heat transfer in tubes and ducts: A review of prandtl number, geometry, and orientation effects. Symmetry, 17(12): 2119. https://doi.org/10.3390/sym17122119
[38] Muralikrishna, Y., Mohan Jagadeesh Kumar, M., Aravind, B., Sahu, M.K. (2023). Comparative studies on performance of plain, perforated, threaded, and threaded–perforated pin fin: A numerical approach. Heat Transfer, 52(4): 3333-3352. https://doi.org/10.1002/htj.22830
[39] Ehsani, H., Roudbari, F.N., Namaghi, S.S., Ganji, D.D. (2024). Investigating thermal performance enhancement in perforated pin fin arrays for cooling electronic systems through integrated CFD and deep learning analysis. Results in Engineering, 22: 102016. https://doi.org/10.1016/j.rineng.2024.102016
[40] Kumar, V., Kumar, R., Gupta, S., Kataria, K.K., Chaudhary, S., Dangi, S. (2024). Enhancement of heat transfer performance of a channel flow using modified delta Winglet vortex generator. Advances in Materials and Processing Technologies, 10(1): 113-119.
[41] Wang, J., Zeng, L., Fu, T., Yu, S., He, Y. (2024). Effects of the position and perforation parameters of the delta winglet vortex generators on flow and heat transfer in minichannels. International Journal of Thermal Sciences, 198: 108878. https://doi.org/10.1016/j.ijthermalsci.2023.108878

NOMENCLATURE

b	Pin-fin base length
c	LVG chord length
C_p	Specific heat capacity
D_h	Hydraulic diameter
f	Friction factor
H	Channel height
h_p	Pin-fin height
k	Thermal conductivity
L	Channel length
Nu	Average Nusselt number
Nu_0	Nusselt number for smooth channel
PEC	Performance evaluation criterion
Pr	Prandtl number
q''	Uniform heat flux
Re	Reynolds number
S_L	Longitudinal pitch
S_T	Transverse pitch
SI	Synergy index
T	Temperature
V_{in}	Inlet bulk velocity
W	Channel width
y^+	Dimensionless wall distance

Greek symbols

α	LVG attack angle
μ	Dynamic viscosity
ρ	Density
ω	Vorticity magnitude
ω^*	Normalized vorticity magnitude ($\omega H/V_{in}$)

Subscripts

0	Smooth channel
avg	Average value
C0	Smooth channel configuration
C1	Perforated triangular pin fins
C2	Longitudinal vortex generators
C3	Combined configuration
in	Inlet
w	Wall